PHILOSOPHICAL TRANSACTIONS A

rsta.royalsocietypublishing.org

Research

Cite this article: Brun P-T, Inamura C, Lizardo D, Franchin G, Stern M, Houk P, Oxman N. 2017 The molten glass sewing machine. *Phil. Trans. R. Soc. A* **375**: 20160156.
http://dx.doi.org/10.1098/rsta.2016.0156

Accepted: 6 December 2016

One contribution of 13 to a theme issue 'Patterning through instabilities in complex media: theory and applications'.

Subject Areas:
mechanical engineering

Keywords:
instability, viscous thread, pattern, coiling, glass, honey

Author for correspondence:
P.-T. Brun
e-mail: pierrethomas.brun@gmail.com

THE ROYAL SOCIETY PUBLISHING

The molten glass sewing machine

P.-T. Brun[1], Chikara Inamura[2], Daniel Lizardo[2], Giorgia Franchin[2,4], Michael Stern[2], Peter Houk[3] and Neri Oxman[2]

[1]Department of Mathematics, [2]Media Lab, and [3]Glass Lab, Department of Materials Science and Engineering, Massachusetts Institute of Technology, Cambridge, MA 02139, USA
[4]Department of Industrial Engineering, University of Padova, 35131 Padova, Italy

P-TB, 0000-0002-4175-0604

We present a fluid-instability-based approach for digitally fabricating geometrically complex uniformly sized structures in molten glass. Formed by mathematically defined and physically characterized instability patterns, such structures are produced via the additive manufacturing of optically transparent glass, and result from the coiling of an extruded glass thread. We propose a minimal geometrical model—and a methodology—to reliably control the morphology of patterns, so that these building blocks can be assembled into larger structures with tailored functionally and optically tunable properties.

This article is part of the themed issue 'Patterning through instabilities in complex media: theory and applications'.

1. Introduction

Since the Bronze Age, humans have put to use the inherent compliance of liquids to shape matter and construct objects. Metal casting, glass blowing—even painting—are all examples of processes where a final construct is obtained following the solidification of an initially liquid phase. In each of those cases, the liquid phase is shaped by a combination of tools and craftsman skills, until solidification is completed. Through history, this concept has matured into a plethora of industrial processes in areas ranging from the polymer industry to metalworking, as well as the glass and food industries. In these areas, fabrication capabilities have progressed via improvements and

optimization of the constraints applied to the liquid phase that is to be transmuted into a desired shape. The term 'constraint'—as used throughout this article—connotes an externally applied factor preventing the natural evolution of the liquid phase: it can be a physical object, like a mould preventing its flow or a piston forcing its extrusion, or an intangible feature of the process acting on the physical properties of the liquid, such as the temperature profile imposed in an oven. Those engineering successes, however, come at the expense of simplicity. Furthermore, as a consequence of their complex multi-physics components, processes are generally largely tuned empirically with compromises between versatility and reproducibility. Here, we propose to explore an alternative route of fabrication, harnessing pattern-forming fluidic instabilities to fabricate structures in complex media.

A mechanical instability describes the natural tendency of a system to destabilize, that is, to depart from an equilibrium position (not necessarily static) towards a bifurcated, qualitatively and quantitatively different state. Euler's *elastica* is a prototypical example of a buckling instability. When quasi-statically increasing the axial loading of a vertical elastic rod clamped at one end and free at the other, one reaches a *critical* value of the load where the rod *suddenly* fails to retain a straight configuration and *spontaneously* buckles into a laterally deformed shape [1]. The straight solution becomes *unstable* and is never observed in practice past the critical buckling load. Traditionally associated with the failure of engineering structures or loss of control in dynamical systems, instabilities are therefore best avoided. As a consequence, the literature on the subject—particularly in the field of theoretical mechanics—focuses on understanding instabilities in order to prevent or minimize their occurrence. Yet, instabilities can contain useful features [2], in particular, regarding the formation of structured materials and surfaces. The most unstable mode of deformation often dominates post-instability dynamics, to the point that it is the only one observed, thereby setting the wavelength λ of the patterns it forms. Examples are many, from the Rayleigh–Taylor instability in a thin liquid film generating a lattice of monodisperse droplets [3], to the wrinkles and dimples formed on elastic membranes [4], which also organize into well-defined patterns. Such features can be harnessed to actively control surface properties, with applications ranging from solar cells [5] to drag reduction [6]. In fluid mechanics, instabilities leading to singularities are routinely used to induce topology changes, e.g. to form droplets from a bulk of fluid, with applications to inkjet printing, spray painting [7] and microfluidics [8]. However, little has been achieved using fluidic instabilities as a design tool: *exploiting the structure arising from the instability in order to fabricate an object*.

This paper focuses on the buckling [9,10] of viscous threads extruded from a nozzle, which, under the action of gravity, form a myriad of patterns when impacting a surface moving relative to the nozzle [11]. These patterns—similar to the coils formed when syrup or honey drizzles onto a breakfast pancake [12]—include alternating loops, meanders and more intricate patterns [13,14]. These patterns are the result of the path traced out by the viscous thread when impacting the surface, which in turn originate from the mismatch between the 'free fall' terminal velocity of the thread and the motion of the surface [13,15–18]. This condition, combined with geometrical arguments, is sufficient to rationalize the formation of patterns under certain conditions (see §3). Embedded in geometry, coiling patterns are indeed found to be generic: they resist changes in the intrinsic mechanical properties of the thread. In particular, similar patterns have been observed when the thread is elastic [19–21]. Here, we illustrate how such fluidic instabilities may be applied to further the capabilities of additive manufacturing.

The advent of freeform fabrication capabilities—such as 3D printing—has critically impacted the design process, with applications ranging from simple, rapid and economic design iterations in laboratories, to the additive manufacturing of complex objects with unprecedented costs, fabrication rate and quality [22]. Here, we explore the possibility of furthering the capabilities of additive manufacturing by harnessing fluidic instabilities. Specifically, we use a 3D printer extruding threads of molten glass [23] with a large offset, thereby inducing buckling in the thread that subsequently yields the fabrication of coiled patterns. A predictive model of the pattern formation associated with the deposition of the thread allows us to *program the instability* in order to freely fabricate structures in molten glass, which are collected after they have cooled

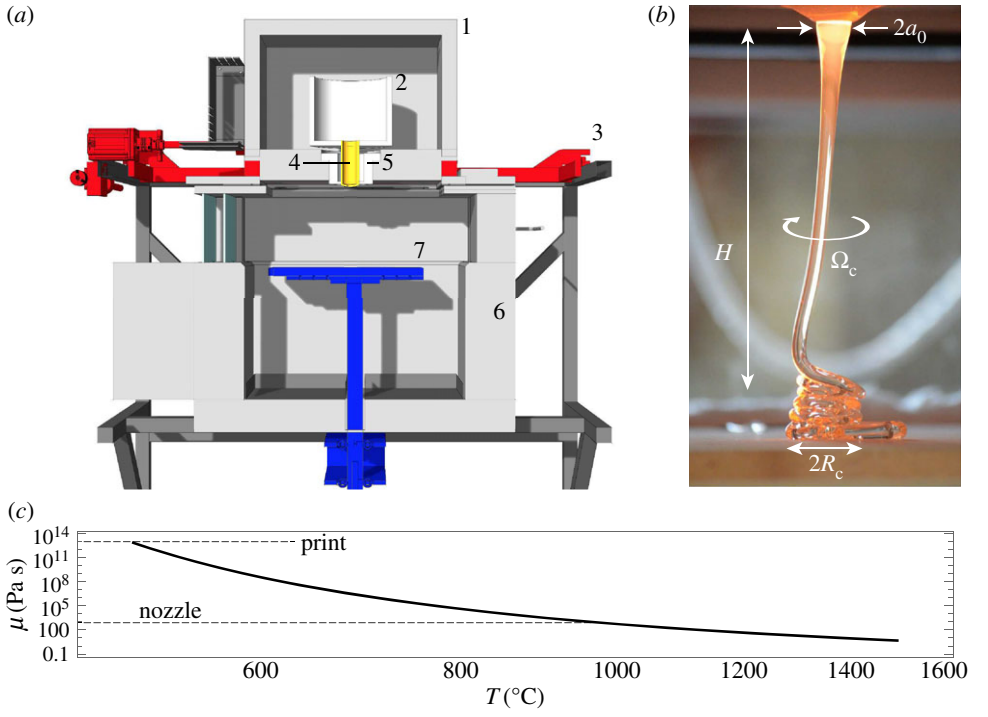

Figure 1. Experimental set-up. (*a*) Schematic view of the 3D printer, which comprises (1) the crucible kiln, (2) crucible, (3) *xy*-motion stage, (4) the nozzle, (5) nozzle kiln, (6) annealing kiln, (7) ceramic build plate and *z*-axis motion. (*b*) Thread of initial radius a_0 falling from a distance H onto the print plate. The thread accelerates under the action of gravity so that its radius decreases during the fall and buckles under its own weight. The coiling motion is characterized by the radius R_c and frequency Ω_c. (*c*) Dynamic viscosity, μ, of the glass thread plotted as a function of temperature as prescribed in equation (2.1), using data from [23]. (Online version in colour.)

down (figure 1*a*,*b*). In stark contrast with the earlier evoked industrial processes, most of the features characterizing the final product—including its characteristic size and shape—do not arise from applied constraints, such as a cast. Rather, they are conveyed *by* the instability, turning this technique into an avenue for freeform fabrication. Specifically, these patterns, whose size exceeds the native resolution of the printer, may be seen as building blocks subsequently assembled into larger structures.

2. A molten glass 3D printer

(a) Set-up

The glass printer shown in figure 1*a* consists of three main heating zones: the crucible kiln that holds the molten glass feedstock (1050°C), the nozzle kiln that heats the nozzle the glass flows through (1010°C) and the annealing kiln that prevents the printed object from cooling too quickly and cracking (500°C). A three-axis computer numeric control (CNC) motion stage is married to the thermal system forming the 3D printer. The motion, precise control of the print height, position and speed of the print head are driven by custom-generated G-code and fed into the stepper motors [23]. For standard operation of the printer, the nozzle is programmed to extrude from one layer height (typically 10 mm) above the previous layer, but for the coiling experiments mentioned in this paper the nozzle is instead spaced at a relatively large offset of 100 mm. By increasing the offset of the printer, its operation could be transformed from traditional 3D

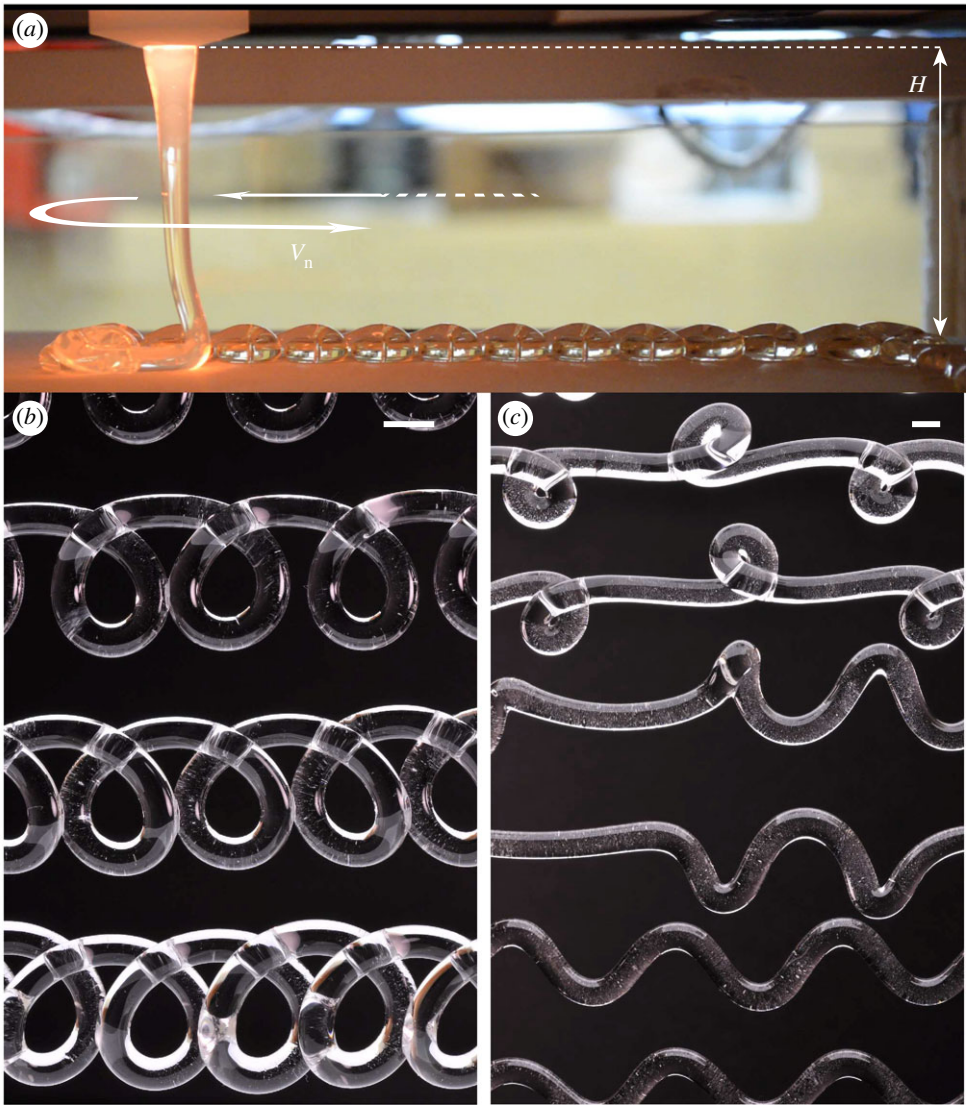

Figure 2. The molten glass sewing machine. (*a*) The nozzle is advected horizontally at speed V_n. Instead of the expected straight line, the system generates a variety of patterns; (*b*) translated coils and (*c*) alternated loops and meanders. Scale bars are 5 mm in length in (*b*) and (*c*). (Online version in colour.)

printing [23] to controlled coil deposition, as discussed in the remainder of this article. For our glass source, we used commercial soda-lime glass (System 96® Studio Nuggets™, Spectrum® Glass Company, Inc., Woodinville, WA, USA). This specific composition is designed for artistic glass-blowing purposes, and thus possesses relatively low softening and annealing points and behaves as a long glass (i.e. it has a wide working temperature window). Nonetheless, the glass dynamic viscosity, μ, strongly depends on temperature, as shown in figure 1*c*, using the Volger–Fulcher–Tammann model:

$$\log \mu(\mathrm{Pa\,s}) = -2.47 + 3964.8/(T(^\circ\mathrm{C}) - 241.5), \tag{2.1}$$

where T denotes the temperature (see [23] for details).

(b) The patterns

In a typical experiment, the value of the offset H—denoting the distance between the nozzle and the print plate—is kept constant, $H \simeq 100$ mm. The nozzle is translated horizontally, progressively mapping the printing surface in the xy-plane at constant speed V_n. Shown in figure 2*a* is the system after one row has been completed and the nozzle is initiating a second row. Here, we have $dx_n(t)/dt = V_n$ and $y_b(t) = C$, where (x_n, y_n) are the coordinates denoting the position of the nozzle and C is a constant that is augmented incrementally after the completion of each row in such a way as to avoid overlap between patterns from adjacent rows. The value of V_n is chosen such that the nozzle is outrun by the terminal speed of the thread right before impact, U_c, i.e. the speed at which glass arrives on the print plate is greater than that of the nozzle lateral motion (see §3). Following [18], we classify patterns using the ratio $V_n/U_c < 1$. We report the existence of three regimes:

— For relatively small advection speeds ($0 < V_n/U_c \lesssim 0.4$), we observe the formation of loops, as evident in figure 2*b*. The spacing between adjacent loops is an increasing function of V_n/U_c, such that for $V_n = 0$ the spacing is effectively zero (figure 1*b*) and is maximal for $V_n/U_c \simeq 0.4$. For instance, in figure 2*b* the nozzle speed incrementally decreases from top to bottom while all other parameters are left constant. As evident from the figure, the distance separating adjacent loops diminishes accordingly.
— For intermediate cases ($0.4 \lesssim V_n/U_c \lesssim 0.6$), we report the formation of tighter loops that appear alternately on one side of the plate and then the other. In figure 2*c*, we show a photograph of these alternating-loop patterns in glass.
— Finally, for speeds V_n approaching U_c ($0.6 \lesssim V_n/U_c \lesssim 1$), those loops open out into meanders (figure 2*c*). Their amplitude is a function of V_n: the closer V_n gets to U_c, the smaller the meanders, such that in the limit—where $V_n = U_c$—we expect meanders to vanish, and the pattern to be straight [13,15]. The straight pattern has not been observed in our experiments, as it is beyond the available speed range of the nozzle.
— We note that for values of $V_n/U_c \simeq 0.7$, i.e. at the transition between meanders and alternating loops, another pattern has been observed. Small loops form only on one side and are connected by a wavy branch (similar to the alternating-loop pattern but without the alternation). Consistent with previous studies, we found that this pattern did not occur often [14,18].

All the aforementioned patterns and their order of appearance are consistent with what is observed in both viscous and elastic cases [19–21]. This robustness suggests the existence of a common explanation for the formation of these patterns, which was recently given in [18,21] and is detailed in the following section so that it may be adapted to molten glass.

3. Pattern design

(a) Geometrical model

We derive a set of equations for the deposition of a thread—represented by its centreline—as it falls from a nozzle translated linearly at speed V_n, and impinges a motionless, flat, solid surface placed at a given distance from the nozzle. The speed at which the thread reaches the plate is denoted $U_c > V_n$. We consider heights of fall small enough so that inertia can be omitted in the problem [18]. Following [18], we assume that U_c is independent of the speed of the nozzle and is thus equal to the coiling speed (i.e. for $V_n = 0$). As a consequence, the path followed by the contact point between thread and plate, $\mathbf{r}(t)$, is directly related to the curvature of the lower end of the thread, κ. In figure 3*a*, we illustrate the behaviour of the end of the thread, which locally acts as a hoop spinning on a table (dashed line aligned to the thread centreline). However, unlike a regular hoop, this virtual hoop has an adaptive curvature κ. Specifically, this radius of curvature

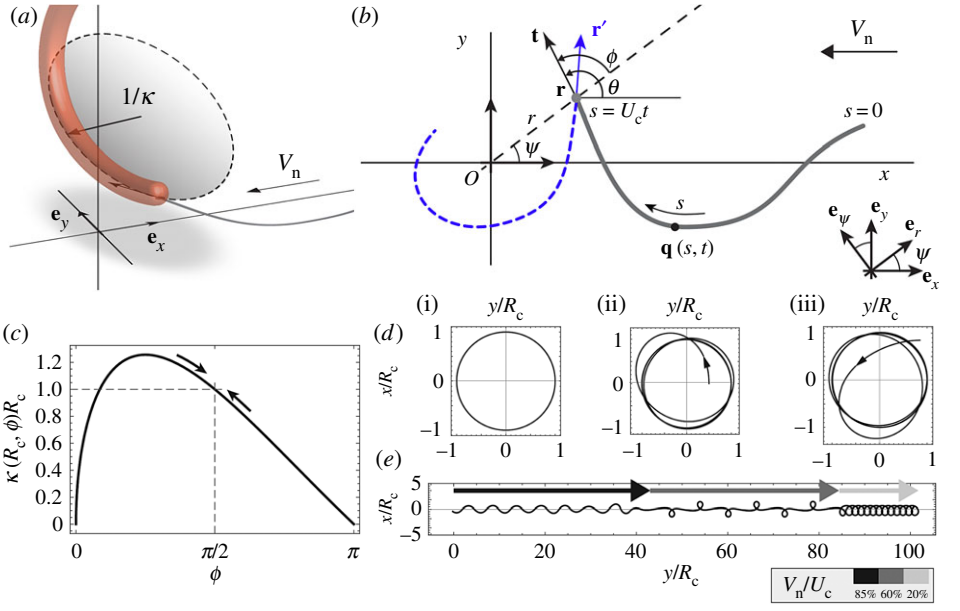

Figure 3. (*a*) Sketch of the heel-like structure of the thread in the vicinity of the printing plate. Its shape is approximated by a fraction of a circle with radius $1/\kappa$. (*b*) Kinematics of the problem describing the position of the contact point, $\mathbf{r}$, and pattern, $\mathbf{q}$, forming at speed U_c while being advected at speed V_n. $\mathbf{t}$ and $\mathbf{r}'$, respectively, denote the tangent to the pattern in the laboratory frame and the tangent to the fictitious trajectory of the contact point in the frame of the nozzle. (*c*) The thread's curvature κ is assumed to be a function of r and ϕ. Shown here is dependence in ϕ for $r = R_c$. (*d*) Integration of the reduced model (3.5) with $V_n = 0$ for (i) $r(0) = 1, \phi(0) = \pi/2$, (ii) $r(0) = 0.5, \phi(0) = \pi/2$ and (iii) $r(0) = 1.2, \phi(0) = 3\pi/4$ displaying the stability of the base solution (i). (*e*) Result of the integration of equation (3.5), where V_n is a piecewise function of time as indicated in the legend. Coils, alternated loops and meanders are recovered. (Online version in colour.)

changes depending on where the thread impinges the plate and its orientation. In the quasi-static regime that we explore, κ is a function of the two state variables of the system: (i) the distance r separating O—the vertical projection of the nozzle on the plate—from the contact point, $\mathbf{r}$; and (ii) the direction followed by the thread as monitored by the angle ϕ between the polar direction $\mathbf{r}$ and the tangent to the pattern $\mathbf{t}$ (figure 3*b*). The curvature κ is *a priori* unknown, aside from the reference case, $V_n = 0$, for which $\kappa = 1/R_c$, where R_c denotes the radius of coiling [10], i.e. the radius of the circular trajectory followed by the thread in figure 1*b*. When $V_n \neq 0$, κ departs from this reference value in such a way as to collapse to a function of (r, ϕ) as demonstrated in [18] in the limit of vanishing inertia. Here, we propose an ansatz for κ with separate variables that captures the essence of the function obtained in [18] while being relatively simpler:

$$\kappa(r,\phi) = \frac{r}{R_c} \sin\left(\pi \sqrt{\frac{|\phi|}{\pi}} \frac{\phi}{|\phi|}\right) \sin\left(\frac{\pi}{\sqrt{2}}\right)^{-1}, \tag{3.1}$$

where R_c is the coiling radius of the thread, that is the adequate length scale of the problem [18]. In figure 3*c*, we illustrate the angular dependence of (3.1) as we plot $\kappa(R_c, \phi)$. Note that for symmetry reasons κ must be odd with respect to ϕ, such that we enforce $\kappa(r, 0) = 0$ and add absolute values to best account for negative values of ϕ. The expression of the curvature in equation (3.1) is tailored such that the system acts in a way analogous to a 'spring' with equilibrium position $r = R_c$, $\phi = \pi/2$. We thus have $\kappa(R_c, \pi/2) = R_c^{-1}$, which describes a circle of radius R_c, in reality corresponding to the coils reported in figure 1*b* for $V_n = 0$. This base solution of the problem is shown in dimensionless units in figure 3*d*(i) and—by design—is stable for, and relevant to, a variety of perturbations when $V_n = 0$, i.e before the symmetry of the problem is broken by

advection of the nozzle. This stabilizing effect, in particular enforced by the square root embedded in the sine in (3.1), is evident in figure 3*c* and is exemplified in figure 3*d*. Outgoing trajectories lead to increased curvatures such that the path returns to a circle (figure 3*d*(ii)). Conversely, converging trajectories have the opposite effect and lead to a decrease of the value of κ, in turn acting so that the system returns to its circular base solution (figure 3*d*(iii)). Note that trajectories in figure 3*d* are drawn at speed U_c, which is the speed at which the thread falls on the printing plate, yielding $|\dot{\mathbf{r}}| = U_c$, where a dot denotes a derivative with respect to time. This equation is the result of the no-slip boundary condition on the plate when $V_n = 0$, and generalizes to

$$U_c \mathbf{t} = \dot{\mathbf{r}} - V_n \mathbf{e}_x, \tag{3.2}$$

when $V_n \neq 0$.

The pattern $\mathbf{q}(s,t)$ represents the position on the printing plate, at time t, of the point of arc-length s. We implicitly define s as the Lagrangian coordinate, such that $s = U_c t^\star$, where $t^\star$ is the time at which the material point s impinges the plate at position $\mathbf{r}(s)$. In the frame of the nozzle, this material point, s, is then advected at velocity $V_n \mathbf{e}_x$ so that its position $\mathbf{q}(s,t)$ at time t is

$$\mathbf{q}(s,t) = \mathbf{r}(s) + V_n \left(t - \frac{s}{U_c} \right) \mathbf{e}_x, \tag{3.3}$$

where the prefactor $t - s/U_c$ denotes the time interval between the current time t and the impact time $t^\star = s/U_c \leq t$. Differentiating equation (3.3) with respect to s and taking its value at $s = U_c t$, we find

$$\mathbf{t}(s) = \left. \frac{\partial \mathbf{q}}{\partial s} \right|_{s = U_c t} = \mathbf{r}'(s) - \frac{V_n}{U_c} \mathbf{e}_x, \tag{3.4}$$

thereby showing that $\dot{\mathbf{r}} = U_c \mathbf{r}'$, when substituting equation (3.4) in equation (3.2). Since the tangent $\mathbf{r}'$ is unitary, we recover that the contact point moves at speed U_c, consistent with our definition of $s = U_c t$.

We now project equation (3.4) in the polar basis $(\mathbf{e}_r, \mathbf{e}_\psi)$ depicted in figure 3*b*, and use the relations $\theta = \psi + \phi$ and $\theta'(s) = \kappa$ to obtain a system of three first-order differential equations:

$$r' = \cos\phi + \frac{V_n}{U_c} \cos\psi, \tag{3.5a}$$

$$r\psi' = \sin\phi - \frac{V_n}{U_c} \sin\psi \tag{3.5b}$$

and

$$\phi' + \psi' = \kappa(r, \phi), \tag{3.5c}$$

where κ is the function defined in equation (3.1). Integrated with an appropriate set of initial conditions (e.g. $r = R_c$, $\phi = \pi/2$ and $\psi = 0$), the system (3.5) yields the patterns reported in figure 3*e*, for which V_n is the piecewise function depicted in the inset. Aside from short transient regimes, the patterns are found to be fully determined by the value of the ratio V_n/U_c, a result that we now take advantage of in practical settings.

(b) Methodology

Our model (3.5) conveys the idea that geometry and kinematics play a central role in pattern formation and in the subsequent morphology. Specifically, we have observed that the nature of the pattern is, in our model, solely determined by the scalar ratio V_n/U_c. This result has practical implications that are discussed next.

In the experiment, the parameter V_n is directly set by the operator, so the only unknown in the problem is effectively U_c. This value can be determined analytically for a Newtonian fluid in steady coiling [10,24,25] or numerically [26] when $V_n \neq 0$. Yet, both methods require knowledge of the fluid's constitutive equations, its Newtonian viscosity, at each point of the thread. In our case, these local physical properties are *a priori* unknown, as they result from the thermal coupling between the thread and the surrounding, cooler, environment. Coupling solutions to the fluid

Figure 4. Comparison between theoretical and experimental results. Experimental photographs of the glass pattern obtained with a nozzle of radius $a_0 = 5$ mm, height of fall $H = 100$ mm and nozzle speed $V_n = [9, 8, 7, 6]$ mm s^{-1} from top to bottom serves as a background of the image. It is compared with the numerical results obtained by integrating equation (3.5) using the values $R_c = 6.8$ mm, $\Omega_c = 2\pi/1.62\,\mathrm{s}^{-1}$, so that $U_c \simeq 26$ mm s^{-1}, and the value of V_n corresponding to each row. The dotted line represents the centreline as predicted by theory, and the transparent orange lines are the result of reconstruction obtained giving adequate thickness to this line in order to best fit the pattern. The scale bar is 5 mm in length. (Online version in colour.)

problem as in [26] to the thermal problem is possible but cumbersome, notably owing to the large temperature gradients in the set-up evident in figure 1*b*. The jet glows next to the nozzle, but this light progressively vanishes along the falling jet. As a consequence, we expect the viscosity to greatly vary, as evident in figure 1*c*.

Instead, we propose to determine U_c experimentally, such that it is benchmarked for a given height of fall in coiling conditions (i.e. $V_n = 0$). For best accuracy we measure the coiling radius R_c and coiling frequency Ω_c, and then use the relation $U_c = R_c\Omega_c$. Such a measurement is easy to implement prior to fabricating patterns, and allows us to accurately determine the time and space scales of the system, which are then used to adjust the nozzle speed accordingly. It is the geometric nature of pattern formation that allows us to 'screen out' the fluidic and thermic components of the problem. Specifically, the boundary layer at the bottom of the thread, responsible for the pattern formation, does not act on U_c: *all the patterns are 'stitched' at the same velocity* [18].

In figure 4, we show the results obtained in our experiments in the case of a thread extruded from a nozzle with a radius $a_0 = 5$ mm and falling from a height $H = 100$ mm. Using images similar to that reported in figure 1*b*, we determine—*once and for all*—that $R_c = 6.8$ mm and $\Omega_c = 2\pi/1.62\,\mathrm{s}^{-1}t$, so that the terminal speed of the filament is $U_c \simeq 26\,\mathrm{mm\,s}^{-1}$. Using the results of our geometric model, we determine the range of nozzle speeds V_n to form coils (typically $V_n \lesssim 0.4U_c$). In figure 4, we show photographs of the glass patterns obtained for $V_n = [9, 8, 7, 6]\,\mathrm{mm\,s}^{-1}$ and compare them with the results of the geometrical model in equation (3.5) integrated *without* adjustable parameters. We identify an agreement between model and experiments, thereby validating the approximations made to derive the model: (i) the quasi-static approximation and geometrical construction (3.5), (ii) the ansatz (3.1), and (iii) the use of a single value for U_c—determined for $V_n = 0$—throughout a range of values of $V_n \neq 0$. Similar results are obtained for meanders and alternating loops (not shown here). Note, however, that our geometrical model,

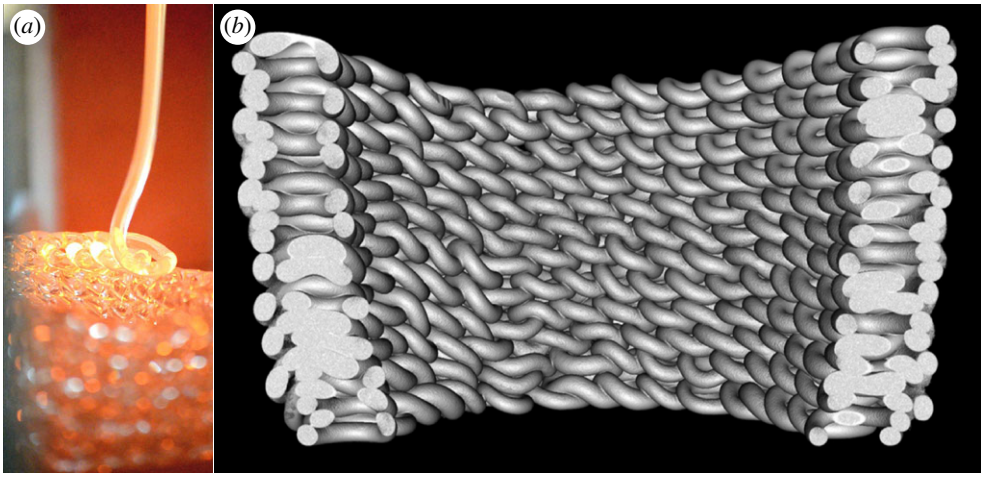

Figure 5. Coiling patterns as building blocks. (*a*) Photograph of an experiment illustrating the structure progressively formed as the nozzle follows a circular printing path. (*b*) Computerized X-ray tomograph scan of the final structure. Each loop is roughly 15 mm in size. (Image credit: James Weaver.) (Online version in colour.)

thus far, solely accounts for the centreline of the thread. Reverting this dimensional reduction, so as to restore a finite thickness in the thread, requires an additional step. This step may be achieved by direct measurement of the thread radius at impact, a_c, or else using mass conservation, yielding $a_c = \sqrt{Q/\pi U_c}$, where Q is the flow rate of the system.

Our geometrical model, coupled to the aforementioned method, may therefore be used to tune the parameters of the experiment, V_n or H, in order to 'program' the thread and drive its buckling instability in a controlled and constructive way. We note the contrast between the simplicity of the nozzle's motion, simply translated at constant speed in the x-direction, and the complexity of the print, which presents features in both the x- and y-directions. This richness is the sole result of the fluidic instability that, in fact, shapes matter through geometrical nonlinearities, thereby *offering an avenue for patterning complex media, such as glass, in a controlled and tunable way*. Here, the coiling instability is used as an instability-assisted design tool, which can be taken advantage of towards the assembly of larger structures.

4. Patterns as building blocks

In this section, we show how coils and other related patterns may be used as building blocks towards the fabrication of larger structures.

Using the settings provided in §3b, we print a piece by moving the nozzle along a circular trajectory with a relatively large radius $R = 50\,\text{mm} \gg R_c$. Upon completion of a circle, the printing plate is lowered to account for the filament thickness, and another circle is made. In figure 5*a*, we show a photograph of the experiment, where the circular path followed by the nozzle is evident. In figure 5*b*, we provide a computerized tomography scan of the resulting structure, which appears as if the glass threads have been 'woven' into a wicker basket. Further, this metaphor becomes instrumental, since each layer presents bonds with adjacent layers, resulting in overall strong mechanical cohesion. We note that those bonds—as well as their distribution—are irregular. This is attributed to the fact that, as a coil forms, it crosses its own path, effectively resulting in the formation of a bump. As a result of this effective roughness, only a fraction of the thread contacts the neighbouring layers. This result contrasts with conventional prints, where a single thread follows the exact path of the nozzle, and where each layer fully bonds with the previous and following layers, strongly stiffening the resulting structure [23]. However, the latter

is more exposed to catastrophic fracture than the former: in its 'woven' configurations, we expect that a mechanical load large enough to damage the structure will lead to a series of small cracks distributed in the wall, as opposed to a single catastrophic fracture crossing the entire structure.

5. Discussion

We have demonstrated the use of a fluidic instability to fabricate systematic patterns in complex media. Specifically, we have shown that coiling-like instability can be harnessed in molten glass as a viable route for fabricating uniformly sized structures. The pattern's morphological features and physical characteristics may be tailored using a single scalar parameter—the nozzle advection speed—when all other parameters remain constant.

The predictive nature of the model proposed is enhanced by the geometrical nature of coiling instability. In the context of this research, the physical properties of the fluid are relevant merely to determine the velocity scale of the system, U_c, denoting the speed at which coils would naturally form when impacting a flat motionless surface. Results achieved are valid within the limit where inertia is negligible, a condition restricted to relatively small heights of fall [10]. Moving to larger heights of fall would broaden the range of accessible patterns [11,13]; however, this development will be made at the expense of the applicability of our model. In such a regime, we expect a coupling between (i) the region near the plate, where patterns are formed, accounted for in our model, and (ii) the vibration modes of the upper section of the flow, where the thread stretches. Incorporating this coupling in our reduced model will be the subject of future work.

In this work, inertia is irrelevant while geometry drives pattern formation. Given this, one would expect that coiling, meandering and alternating-loop patterns would form in settings whose typical size is significantly smaller than those explored and included within this paper (and to some extent in low-Reynolds-number microfluidic settings [27,28]).

This is indeed the case—as shown in [29,30], where coils with approximate radius of 50 µm have been obtained via coiling with the goal of fabricating microstructures featuring sacrificial bonds. This avenue of research—inspired by natural materials constructed in a hierarchical manner—could benefit from the predictive nature of our model, which, *in fine*, permits the fabrication of regularly sized structures in complex media and their assembly without the need for external assistance. Such salutary features may be taken advantage of in the additive manufacturing of cellular structures [31]. In this context, glass—as a chemically inert, optically transparent, mechanically strong material—has great potential for future applications ranging from design and architecture to the digital fabrication of bio-compatible and even bio-augmented scaffolds. Finally, coiling is demonstrated as a method to rapidly fabricate and assemble tailored structures at a scale exceeding the native resolution of the printer.

Data accessibility. All the data discussed in the article are readily available in the publication.

Authors' contributions. P.-T.B. and N.O. have designed the research. C.I., D.L., G.F., M.S. and P.H. performed the experiments. P.-T.B. provided the model and wrote the paper.

Competing interests. C.I., D.L., G.F., M.S., P.H. and N.O. have filed a US Patent Application No. 14697564 on 27 April 2015. No other competing financial interests exist.

Funding. The research was primarily sponsored by the Mediated Matter research group at the MIT Media Lab. It was supported in part by the MIT Department of Mechanical Engineering through a project in the course 'Additive manufacturing' (2.S998) in spring 2014 and by the Glass Art Society through the Technology Advancing Glass Grant. G.F. was partially supported by a scholarship awarded by 'Fondazione Aldo Gini' in Padova, Italy.

Acknowledgements. We thank Associate Prof. John A. Hart for his support of our work and for his technical advice. We also thank Prof. J. Meejin Yoon, Department Head and MIT's School of Architecture and Planning, as well as Prof. John A. Ochsendorf from MIT's Department of Civil and Environmental Engineering and Prof. Neil Gershenfeld from MIT's Center for Bits and Atoms for their guidance and support. We thank James Weaver for collecting the image used in figure 5*b*; Mary Ann Babula for cutting, grinding and polishing; Michael Tarkanian and Daniel Lizardo for their assistance. We also wish to acknowledge Corning Incorporated for viscosity measurements and technical advice, as well as Skutt Kilns and Smart Ceramics

for support during the printer design and building phases. In addition, we thank Joi Ito, director of the MIT Media Lab, for his continuous support.

References

1. Audoly B, Pomeau Y. 2010 *Elasticity and geometry: from hair curls to the non-linear response of shells*. Oxford, UK: Oxford University Press.
2. PM Reis. 2015 A perspective on the revival of structural (in)stability with novel opportunities for function: from buckliphobia to buckliphilia. *J. Appl. Mech.* **82**, 111001. (doi:10.1115/1.4031456)
3. Fermigier M, Limat L, Wesfreid JE, Boudinet P, Quilliet C. 1992 Two-dimensional patterns in Rayleigh–Taylor instability of a thin layer. *J. Fluid Mech.* **236**, 349–383. (doi:10.1017/S0022112092001447)
4. Cao Y, Hutchinson JW. 2012 From wrinkles to creases in elastomers: the instability and imperfection-sensitivity of wrinkling. *Proc. R. Soc. A* **468**, 94–115. (doi:10.1098/rspa.2011.0384)
5. Kim JB, Kim P, Pégard NC, Oh SJ, Kagan CR, Fleischer JW, Stone HA, Loo Y-L. 2012 Wrinkles and deep folds as photonic structures in photovoltaics. *Nat. Photon.* **6**, 327–332. (doi:10.1038/nphoton.2012.70)
6. Terwagne D, Brojan M, Reis PM. 2014 Smart morphable surfaces for aerodynamic drag control. *Adv. Mater.* **26**, 6608–6611. (doi:10.1002/adma.201401403)
7. Eggers J, Villermaux E. 2008 Physics of liquid jets. *Rep. Prog. Phys.* **71**, 036601. (doi:10.1088/0034-4885/71/3/036601)
8. Baroud CN, Gallaire F, Dangla R. 2010 Dynamics of microfluidic droplets. *Lab Chip* **10**, 2032–2045. (doi:10.1039/c001191f)
9. Taylor GI 1969 Instability of jets, threads, and sheets of viscous fluid. In *Applied mechanics*, pp. 382–388. Berlin, Germany: Springer.
10. Ribe NM, Habibi M, Bonn D. 2012 Liquid rope coiling. *Annu. Rev. Fluid Mech.* **44**, 249–266. (doi:10.1146/annurev-fluid-120710-101244)
11. Chiu-Webster S, Lister JR. 2006 The fall of a viscous thread onto a moving surface: a 'fluid-mechanical sewing machine'. *J. Fluid Mech.* **569**, 89–111. (doi:10.1017/S0022112006002503)
12. Mahadevan L, Ryu WS, Samuel ADT. 1998 Fluid 'rope trick' investigated. *Nature* **392**, 140. (doi:10.1038/32321)
13. Morris SW, Dawes JHP, Ribe NM, Lister JR. 2008 Meandering instability of a viscous thread. *Phys. Rev. E* **77**, 066218. (doi:10.1103/PhysRevE.77.066218)
14. Welch RL, Szeto B, Morris SW. 2012 Frequency structure of the nonlinear instability of a dragged viscous thread. *Phys. Rev. E* **85**, 066209. (doi:10.1103/PhysRevE.85.066209)
15. Ribe NM, Lister JR, Chiu-Webster S. 2006 Stability of a dragged viscous thread: onset of 'stitching' in a fluid-mechanical 'sewing machine'. *Phys. Fluids* **18**, 124105. (doi:10.1063/1.2409617)
16. Blount MJ, Lister JR. 2011 The asymptotic structure of a slender dragged viscous thread. *J. Fluid Mech.* **674**, 489–521. (doi:10.1017/S0022112011000085)
17. Brun P-T, Ribe NM, Audoly B. 2012 A numerical investigation of the fluid mechanical sewing machine. *Phys. Fluids* **24**, 043102. (doi:10.1063/1.3703316)
18. Brun P-T, Audoly B, Ribe NM, Eaves TS, Lister JR. 2015 Liquid ropes: a geometrical model for thin viscous jet instabilities. *Phys. Rev. Lett.* **114**, 174501. (doi:10.1103/PhysRevLett.114.174501)
19. Habibi M, Najafi J, Ribe NM. 2011 Pattern formation in a thread falling onto a moving belt: an 'elastic sewing machine'. *Phys. Rev. E* **84**, 016219. (doi:10.1103/PhysRevE.84.016219)
20. Jawed MK, Da F, Joo J, Grinspun E, Reis PM. 2014 Coiling of elastic rods on rigid substrates. *Proc. Natl Acad. Sci. USA* **111**, 14 663–14 668. (doi:10.1073/pnas.1409118111)
21. Jawed MK, Brun P-T, Reis PM. 2015 A geometric model for the coiling of an elastic rod deployed onto a moving substrate. *J. Appl. Mech.* **82**, 121007. (doi:10.1115/1.4031363)
22. Gibson I, Rosen DW, Stucker B. 2010 *Additive manufacturing technologies: Rapid prototyping to direct digital manufacturing*. Berlin, Germany: Springer. (doi:10.1007/978-1-4419-1120-9)
23. Klein J *et al.* 2015 Additive manufacturing of optically transparent glass. *3D Print. Addit. Manuf.* **2**, 92–105. (doi:10.1089/3dp.2015.0021)
24. Ribe NM. 2004 Coiling of viscous jets. *Proc. R. Soc. Lond. A* **460**, 3223–3239. (doi:10.1098/rspa.2004.1353)

25. Ribe NM, Huppert HE, Hallworth MA, Habibi M, Bonn D. 2006 Multiple coexisting states of liquid rope coiling. *J. Fluid Mech.* **555**, 275–297. (doi:10.1017/S0022112006009153)
26. Audoly B, Clauvelin N, Brun P-T, Bergou M, Grinspun E, Wardetzky M. 2013 A discrete geometric approach for simulating the dynamics of thin viscous threads. *J. Comput. Phys.* **253**, 18–49. (doi:10.1016/j.jcp.2013.06.034)
27. Cubaud T, Jose BM, Darvishi S. 2011 Folded micro-threads: role of viscosity and interfacial tension. *Phys. Fluids* **23**, 042002. (doi:10.1063/1.3573383)
28. Nunes JK, Constantin H, Stone HA. 2013 Microfluidic tailoring of the two-dimensional morphology of crimped microfibers. *Soft Matter* **9**, 4227–4235. (doi:10.1039/c3sm27579e)
29. Guo S-Z, Gosselin F, Guerin N, Lanouette A-M, Heuzey M-C, Therriault D. 2013 Solvent-cast three-dimensional printing of multifunctional microsystems. *Small* **9**, 4118–4122. (doi:10.1002/smll.201300975)
30. Passieux R, Guthrie L, Rad SH, Lévesque M, Therriault D, Gosselin FP. 2015 Instability-assisted direct writing of microstructured fibers featuring sacrificial bonds. *Adv. Mater.* **27**, 3676–3680. (doi:10.1002/adma.201500603)
31. Lipton JI, Lipson H. 2016 3D printing variable stiffness foams using viscous thread instability. *Sci. Rep.* **6**, 29996. (doi:10.1038/srep29996)